

# The exact equivalence of the two-flavour strong coupling lattice Schwinger model with Wilson fermions to a vertex model

K. Scharnhorst<sup>†</sup>

University of Wales, Swansea  
Department of Physics  
Singleton Park  
Swansea, SA2 8PP, U.K.

## Abstract

In this paper a method previously employed by Salmhofer to establish an exact equivalence of the one-flavour strong coupling lattice Schwinger model with Wilson fermions to some 8-vertex model is applied to the case with two flavours. As this method is fairly general and can be applied to strong coupling QED and purely fermionic models with any (sufficiently small) number of Wilson fermions in any dimension the purpose of the present study is mainly a methodical one in order to gain some further experience with it. In the paper the vertex model equivalent to the two-flavour strong coupling lattice Schwinger model with Wilson fermions is found. It turns out to be some modified 3-state 20-vertex model on the square lattice, which can also be understood as a regular 6-state vertex model. In analogy with the one-flavour case, this model can be viewed as some loop model.

---

<sup>†</sup>E-mail: k.scharnhorst @ swansea.ac.uk

The motivation for the present work derives from a paper by Salmhofer [1] who demonstrated the exact equivalence of the one-flavour strong coupling lattice Schwinger model with Wilson fermions to a 8-vertex model which can also be understood as a certain self-avoiding loop model. While strongly coupled gauge theories with staggered fermions lead to pure monomer-dimer systems [2] the consideration of Wilson fermions results in more complicated models, as the investigation of Salmhofer [1] demonstrates by example. The particular equivalence established by him has led to hitherto unfeasible computer studies [3]–[5] as well as to the application of certain analytical methods [6] yielding previously unknown information about the critical behaviour of the one-flavour strong coupling lattice Schwinger model. However, the method employed by Salmhofer [1] is not specific to this model. It can equally be applied, under certain technical complications, to strong coupling lattice QED (in fact, to any gauge theory, with some modifications) and purely fermionic models with any (sufficiently small) number of Wilson fermions in any dimension. It is therefore particularly interesting for models with an odd number of fermion species which give rise to serious difficulties for any numerical simulation so far. Furthermore, the vertex model equivalence (which has to be found case by case) of certain lattice models of quantum field theory with Wilson fermions possibly will allow to make use of cluster algorithms for their numerical study in order to reduce the computational effort required. Beyond this, the equivalence may also lead to new ideas for analytical investigations.

In this paper we extend the analysis of Salmhofer [1] to the two-flavour strong coupling lattice Schwinger model. Beyond the specific result of the paper – the vertex model equivalence for the model under consideration – the main purpose of it is to collect some practical experience in dealing with models which have a larger number of Grassmann variables per lattice site than the one-flavour Schwinger model with Wilson fermions, which has four. The main difficulty is an algebraic one. While the study of Salmhofer [1] requires paper and pencil only, to go beyond becomes possible only by using an appropriate formula manipulation program. In this study we are using a program for Mathematica [7] which can efficiently handle Grassmann variables and which has been designed just for the present purpose.

Before going into technical details, let us shortly describe the method to be used in words [1]. The square lattice  $\Lambda$  the two-flavour Schwinger model is defined on is divided into an even and an odd sublattice. Use will be made of the fact that effectively only fermionic degrees of freedom are left in the theory under consideration (In the strong coupling Schwinger model the bosonic gauge field degrees of freedom are integrated out exactly first, leaving the fermionic sector for further consideration.). First, on the (say) even sublattice  $\Lambda_e$  the Grassmann integration is carried out. This is a local procedure (the reason for it being, that at most nearest-neighbour cou-

plings are present in the action) which amounts to a completely algebraic problem due to the Grassmannian character of the integration. The remaining Grassmann variables live on the odd sublattice  $\Lambda_o$  and certain graphical rules, i.e. vertices, can be assigned to their combinations in a fairly natural way. In the final step an analysis can then be made what structures (lattice clusters) built of these vertices the remaining Grassmannian integration on the odd sublattice leads to. Since for Wilson fermions the lattice is homogeneous the result can be described in terms of a vertex model.

We are now prepared to pursue the program for the two-flavour Schwinger model with Wilson fermions (with Wilson parameter  $r = 1$ ). For easier reference, our notation follows closely that applied in [1]. The partition function  $Z_\Lambda$  of the model on the square lattice  $\Lambda$  is given by

$$Z_\Lambda = \int DU \prod_{i=1}^2 D\psi_i D\bar{\psi}_i e^{-S} \quad , \quad (1)$$

where  $D\psi_i D\bar{\psi}_i = \prod_{x \in \Lambda} \prod_{\alpha=1}^2 d\psi_{i,\alpha}(x) d\bar{\psi}_{i,\alpha}(x)$  denotes the multiple Grassmann integration on the lattice ( $i$  is the flavour index.). The action  $S$  is defined by

$$S = S_F + \beta S_G \quad , \quad (2)$$

$$S_F = \sum_{x \in \Lambda} \sum_{i=1}^2 \left( \frac{1}{2} \sum_{\mu} \left( \bar{\psi}_i(x + e_\mu) (1 + \gamma_\mu) U_\mu(x) \psi_i(x) \right. \right. \\ \left. \left. + \bar{\psi}_i(x) (1 - \gamma_\mu) U_\mu^\dagger(x) \psi_i(x + e_\mu) \right) - M_i \bar{\psi}_i(x) \psi_i(x) \right) \quad , \quad (3)$$

and  $U_\mu = \exp[-iA_\mu]$ ,  $\beta = 1/g^2$ .  $S_G$  is the standard Wilson action and the hopping parameters  $\kappa_i$  are given by  $\kappa_i = 1/2M_i$  (For the sake of generality we allow for different masses for each flavour here.). In the strong (infinite) coupling limit  $\beta = 0$  the gauge field integration can be performed exactly and one finds (cf. eq. (5) in [1])

$$Z_\Lambda = \sum_{k_l \in \{0,1,2,3,4\}} \int \prod_{i=1}^2 D\psi_i D\bar{\psi}_i \exp \left( \sum_{x \in \Lambda} \sum_{j=1}^2 M_j \bar{\psi}_j(x) \psi_j(x) \right) \\ \times \prod_{l=(x,x+e_\mu)} \frac{1}{k_l! 2^{k_l}} \left[ \left( \sum_{m=1}^2 \bar{\psi}_m(x) T_\mu^{(-)} \psi_m(x + e_\mu) \right) \left( \sum_{n=1}^2 \bar{\psi}_n(x + e_\mu) T_\mu^{(+)} \psi_n(x) \right) \right]^{k_l} . \quad (4)$$

In the two-flavour Schwinger model, the occupation numbers  $k_l$  cannot exceed 4 because on each lattice site only 8 Grassmann variables are present. In fact, explicit calculation shows that by virtue of the nilpotency of the Grassmann variables  $k_l$  cannot exceed 2. As in [1], we choose  $\gamma_1 = \sigma_3$ ,  $\gamma_2 = \sigma_1$  ( $\sigma_i$  are Pauli matrices.) and the projection operators  $T_\mu^{(\epsilon)} = (1 + \epsilon\gamma_\mu)/2$ ,  $\epsilon \in \{-1, 1\}$  then read  $T_1^{(+)} = \text{diag}\{1, 0\}$ ,  $T_1^{(-)} = \text{diag}\{0, 1\}$ ,  $T_2^{(\epsilon)} = \frac{1}{2} \begin{pmatrix} 1 & \epsilon \\ \epsilon & 1 \end{pmatrix}$ . It is now advantageous in order to simplify further results to define for each flavour combinations of the original  $\psi$  fields in which terms  $T_2^{(\epsilon)}$  is diagonal (The index in front of the comma always is the flavour index, the one behind it the component index.)

$$\chi_i(x) = U\psi_i(x) = \frac{1}{\sqrt{2}} (\psi_{i,1}(x) + \psi_{i,2}(x), \psi_{i,1}(x) - \psi_{i,2}(x))^T \quad , \quad (5)$$

$$\bar{\chi}_i(x) = \bar{\psi}_i(x)U = \frac{1}{\sqrt{2}} (\bar{\psi}_{i,1}(x) + \bar{\psi}_{i,2}(x), \bar{\psi}_{i,1}(x) - \bar{\psi}_{i,2}(x)) \quad (6)$$

with

$$U = \frac{1}{\sqrt{2}} \begin{pmatrix} 1 & 1 \\ 1 & -1 \end{pmatrix} = U^{-1} \quad . \quad (7)$$

In the expression for the partition function (4) the integration on the even sublattice  $\Lambda_e$  is now performed first. As each lattice site  $x$  supports 8 Grassmann variables terms which respect

$$\sum_{l \ni x} k_l + s_x = 4 \quad (8)$$

can give a non-vanishing contribution only ( $s_x$  is the power of  $\sum_{i=1}^2 M_i \bar{\psi}_i(x) \psi_i(x)$  in eq. (4).). Explicit calculation now reveals that only terms with  $s_x = 0$  or  $s_x = 4$  are non-vanishing. A given set of  $k_l$  on the lattice  $\Lambda$  uniquely determines a certain configuration contributing to the partition function. Below we give the results for all local integrals related to a given lattice site  $x \in \Lambda_e$  which allow non-vanishing contributions. The results have been arranged in a way most suitable for the further discussion. While in [1] the calculation for the one-flavour model has been performed by means of paper and pencil, the two-flavour case requires use of the computer and we have relied on a purpose-written Mathematica program [7] to do the necessary algebra. The graphical rules below have to be interpreted as follows: the black dot denotes any point  $x$  on the even sublattice  $\Lambda_e$  at which the Grassmann integration is performed, a dashed line means  $k_l = 0$  while thin and thick lines stand for  $k_l = 1$  and  $k_l = 2$  respectively. The first coordinate component of

$x$  is understood to be the horizontal one while the second component runs vertically.

There is one possible vertex with  $s_x = 4$ :

Vertex 1

$$\begin{aligned}
 \text{---} \cdot \text{---} &= \int \prod_{i=1}^2 \prod_{\alpha=1}^2 d\psi_{i,\alpha}(x) d\bar{\psi}_{i,\alpha}(x) \frac{1}{4!} \left( \sum_{i=1}^2 M_i \bar{\psi}_i(x) \psi_i(x) \right)^4 \\
 &= M_1^2 M_2^2
 \end{aligned} \tag{9}$$

All further vertices have  $s_x = 0$  of course.

Vertex 2

$$\begin{aligned}
 \text{---} \perp \text{---} &= \bar{\chi}_{1,1}(x + e_2) \bar{\chi}_{2,2}(x - e_2) \bar{\chi}_{1,2}(x - e_2) \bar{\chi}_{2,1}(x + e_2) \\
 &\times \chi_{1,2}(x + e_2) \chi_{2,1}(x - e_2) \chi_{1,1}(x - e_2) \chi_{2,2}(x + e_2)
 \end{aligned} \tag{10}$$

Vertex 3

$$\begin{aligned}
 \perp \text{---} &= \bar{\psi}_{1,1}(x + e_1) \bar{\psi}_{2,2}(x - e_1) \bar{\psi}_{1,2}(x - e_1) \bar{\psi}_{2,1}(x + e_1) \\
 &\times \psi_{1,2}(x + e_1) \psi_{2,1}(x - e_1) \psi_{1,1}(x - e_1) \psi_{2,2}(x + e_1)
 \end{aligned} \tag{11}$$

Vertex 4

$$\begin{aligned}
 \text{---} \perp &= \bar{\chi}_{1,2}(x - e_2) \bar{\psi}_{2,1}(x + e_1) \bar{\psi}_{1,1}(x + e_1) \bar{\chi}_{2,2}(x - e_2) \\
 &\times \chi_{1,1}(x - e_2) \psi_{2,2}(x + e_1) \psi_{1,2}(x + e_1) \chi_{2,1}(x - e_2)/4
 \end{aligned} \tag{12}$$

Vertex 5

$$\begin{aligned}
 \perp \text{---} &= \bar{\chi}_{1,1}(x + e_2) \bar{\psi}_{2,2}(x - e_1) \bar{\psi}_{1,2}(x - e_1) \bar{\chi}_{2,1}(x + e_2) \\
 &\times \chi_{1,2}(x + e_2) \psi_{2,1}(x - e_1) \psi_{1,1}(x - e_1) \chi_{2,2}(x + e_2)/4
 \end{aligned} \tag{13}$$

Vertex 6

$$\begin{array}{c} \text{---} \perp \text{---} \\ | \\ \text{---} \end{array} = \bar{\chi}_{1,1}(x+e_2) \bar{\psi}_{2,1}(x+e_1) \bar{\psi}_{1,1}(x+e_1) \bar{\chi}_{2,1}(x+e_2) \\ \times \chi_{1,2}(x+e_2) \psi_{2,2}(x+e_1) \psi_{1,2}(x+e_1) \chi_{2,2}(x+e_2)/4 \quad (14)$$

Vertex 7

$$\begin{array}{c} | \\ \text{---} \perp \text{---} \\ \text{---} \end{array} = \bar{\chi}_{1,2}(x-e_2) \bar{\psi}_{2,2}(x-e_1) \bar{\psi}_{1,2}(x-e_1) \bar{\chi}_{2,2}(x-e_2) \\ \times \chi_{1,1}(x-e_2) \psi_{2,1}(x-e_1) \psi_{1,1}(x-e_1) \chi_{2,1}(x-e_2)/4 \quad (15)$$

Vertex 8

$$\begin{array}{c} | \\ \text{---} \perp \text{---} \\ | \end{array} = - \left[ \bar{\chi}_{1,1}(x+e_2) \bar{\chi}_{2,2}(x-e_2) + \bar{\chi}_{1,2}(x-e_2) \bar{\chi}_{2,1}(x+e_2) \right] \\ \times \left[ \chi_{1,2}(x+e_2) \chi_{2,1}(x-e_2) + \chi_{1,1}(x-e_2) \chi_{2,2}(x+e_2) \right] \\ \times \bar{\psi}_{1,2}(x-e_1) \bar{\psi}_{2,2}(x-e_1) \psi_{1,1}(x-e_1) \psi_{2,1}(x-e_1)/4 \quad (16)$$

Vertex 9

$$\begin{array}{c} \text{---} \perp \text{---} \\ | \\ \text{---} \end{array} = - \left[ \bar{\chi}_{1,1}(x+e_2) \bar{\chi}_{2,2}(x-e_2) + \bar{\chi}_{1,2}(x-e_2) \bar{\chi}_{2,1}(x+e_2) \right] \\ \times \left[ \chi_{1,2}(x+e_2) \chi_{2,1}(x-e_2) + \chi_{1,1}(x-e_2) \chi_{2,2}(x+e_2) \right] \\ \times \bar{\psi}_{1,1}(x+e_1) \bar{\psi}_{2,1}(x+e_1) \psi_{1,2}(x+e_1) \psi_{2,2}(x+e_1)/4 \quad (17)$$

Vertex 10

$$\begin{array}{c} | \\ \text{---} \perp \text{---} \\ | \end{array} = - \left[ \bar{\psi}_{1,1}(x+e_1) \bar{\psi}_{2,2}(x-e_1) + \bar{\psi}_{1,2}(x-e_1) \bar{\psi}_{2,1}(x+e_1) \right] \\ \times \left[ \psi_{1,2}(x+e_1) \psi_{2,1}(x-e_1) + \psi_{1,1}(x-e_1) \psi_{2,2}(x+e_1) \right] \\ \times \bar{\chi}_{1,1}(x+e_2) \bar{\chi}_{2,1}(x+e_2) \chi_{1,2}(x+e_2) \chi_{2,2}(x+e_2)/4 \quad (18)$$

Vertex 11

$$\begin{array}{c} | \\ \text{---} \perp \text{---} \\ | \end{array} = - \left[ \bar{\psi}_{1,1}(x+e_1) \bar{\psi}_{2,2}(x-e_1) + \bar{\psi}_{1,2}(x-e_1) \bar{\psi}_{2,1}(x+e_1) \right] \\ \times \left[ \psi_{1,2}(x+e_1) \psi_{2,1}(x-e_1) + \psi_{1,1}(x-e_1) \psi_{2,2}(x+e_1) \right] \\ \times \bar{\chi}_{1,2}(x-e_2) \bar{\chi}_{2,2}(x-e_2) \chi_{1,1}(x-e_2) \chi_{2,1}(x-e_2)/4 \quad (19)$$

Vertex 12

$$\begin{aligned}
 \begin{array}{c} \vdots \\ \text{---} \bullet \text{---} \\ \vdots \end{array} &= \begin{aligned} & \left[ \bar{\chi}_{1,2}(x - e_2) \bar{\psi}_{2,1}(x + e_1) + \bar{\psi}_{1,1}(x + e_1) \bar{\chi}_{2,2}(x - e_2) \right] \\ & \times \left[ \chi_{1,1}(x - e_2) \psi_{2,2}(x + e_1) + \psi_{1,2}(x + e_1) \chi_{2,1}(x - e_2) \right] \\ & \times \bar{\psi}_{1,2}(x - e_1) \bar{\psi}_{2,2}(x - e_1) \psi_{1,1}(x - e_1) \psi_{2,1}(x - e_1)/2 \end{aligned} \quad (20)
 \end{aligned}$$

Vertex 13

$$\begin{aligned}
 \begin{array}{c} \vdots \\ \text{---} \bullet \text{---} \\ \vdots \end{array} &= \begin{aligned} & \left[ \bar{\chi}_{1,2}(x - e_2) \bar{\psi}_{2,1}(x + e_1) + \bar{\psi}_{1,1}(x + e_1) \bar{\chi}_{2,2}(x - e_2) \right] \\ & \times \left[ \chi_{1,1}(x - e_2) \psi_{2,2}(x + e_1) + \psi_{1,2}(x + e_1) \chi_{2,1}(x - e_2) \right] \\ & \times \bar{\chi}_{1,1}(x + e_2) \bar{\chi}_{2,1}(x + e_2) \chi_{1,2}(x + e_2) \chi_{2,2}(x + e_2)/2 \end{aligned} \quad (21)
 \end{aligned}$$

Vertex 14

$$\begin{aligned}
 \begin{array}{c} \vdots \\ \text{---} \bullet \text{---} \\ \vdots \end{array} &= \begin{aligned} & \left[ \bar{\chi}_{1,1}(x + e_2) \bar{\psi}_{2,2}(x - e_1) + \bar{\psi}_{1,2}(x - e_1) \bar{\chi}_{2,1}(x + e_2) \right] \\ & \times \left[ \chi_{1,2}(x + e_2) \psi_{2,1}(x - e_1) + \psi_{1,1}(x - e_1) \chi_{2,2}(x + e_2) \right] \\ & \times \bar{\psi}_{1,1}(x + e_1) \bar{\psi}_{2,1}(x + e_1) \psi_{1,2}(x + e_1) \psi_{2,2}(x + e_1)/2 \end{aligned} \quad (22)
 \end{aligned}$$

Vertex 15

$$\begin{aligned}
 \begin{array}{c} \vdots \\ \text{---} \bullet \text{---} \\ \vdots \end{array} &= \begin{aligned} & \left[ \bar{\chi}_{1,1}(x + e_2) \bar{\psi}_{2,2}(x - e_1) + \bar{\psi}_{1,2}(x - e_1) \bar{\chi}_{2,1}(x + e_2) \right] \\ & \times \left[ \chi_{1,2}(x + e_2) \psi_{2,1}(x - e_1) + \psi_{1,1}(x - e_1) \chi_{2,2}(x + e_2) \right] \\ & \times \bar{\chi}_{1,2}(x - e_2) \bar{\chi}_{2,2}(x - e_2) \chi_{1,1}(x - e_2) \chi_{2,1}(x - e_2)/2 \end{aligned} \quad (23)
 \end{aligned}$$

Vertex 16

$$\begin{aligned}
 \begin{array}{c} \vdots \\ \text{---} \bullet \text{---} \\ \vdots \end{array} &= - \begin{aligned} & \left[ \bar{\psi}_{1,1}(x + e_1) \bar{\chi}_{2,1}(x + e_2) + \bar{\chi}_{1,1}(x + e_2) \bar{\psi}_{2,1}(x + e_1) \right] \\ & \times \left[ \psi_{1,2}(x + e_1) \chi_{2,2}(x + e_2) + \chi_{1,2}(x + e_2) \psi_{2,2}(x + e_1) \right] \\ & \times \bar{\psi}_{1,2}(x - e_1) \bar{\psi}_{2,2}(x - e_1) \psi_{1,1}(x - e_1) \psi_{2,1}(x - e_1)/2 \end{aligned} \quad (24)
 \end{aligned}$$

Vertex 17

$$\begin{aligned}
 \begin{array}{c} | \\ \text{---} \text{---} \text{---} \\ | \end{array} &= - \left[ \bar{\psi}_{1,1}(x+e_1) \bar{\chi}_{2,1}(x+e_2) + \bar{\chi}_{1,1}(x+e_2) \bar{\psi}_{2,1}(x+e_1) \right] \\
 &\times \left[ \psi_{1,2}(x+e_1) \chi_{2,2}(x+e_2) + \chi_{1,2}(x+e_2) \psi_{2,2}(x+e_1) \right] \\
 &\times \bar{\chi}_{1,2}(x-e_2) \bar{\chi}_{2,2}(x-e_2) \chi_{1,1}(x-e_2) \chi_{2,1}(x-e_2)/2 \quad (25)
 \end{aligned}$$

Vertex 18

$$\begin{aligned}
 \begin{array}{c} | \\ | \text{---} \text{---} \text{---} \\ | \end{array} &= - \left[ \bar{\psi}_{1,2}(x-e_1) \bar{\chi}_{2,2}(x-e_2) + \bar{\chi}_{1,2}(x-e_2) \bar{\psi}_{2,2}(x-e_1) \right] \\
 &\times \left[ \psi_{1,1}(x-e_1) \chi_{2,1}(x-e_2) + \chi_{1,1}(x-e_2) \psi_{2,1}(x-e_1) \right] \\
 &\times \bar{\chi}_{1,1}(x+e_2) \bar{\chi}_{2,1}(x+e_2) \chi_{1,2}(x+e_2) \chi_{2,2}(x+e_2)/2 \quad (26)
 \end{aligned}$$

Vertex 19

$$\begin{aligned}
 \begin{array}{c} | \\ | \text{---} \text{---} \text{---} \\ | \end{array} &= - \left[ \bar{\psi}_{1,2}(x-e_1) \bar{\chi}_{2,2}(x-e_2) + \bar{\chi}_{1,2}(x-e_2) \bar{\psi}_{2,2}(x-e_1) \right] \\
 &\times \left[ \psi_{1,1}(x-e_1) \chi_{2,1}(x-e_2) + \chi_{1,1}(x-e_2) \psi_{2,1}(x-e_1) \right] \\
 &\times \bar{\psi}_{1,1}(x+e_1) \bar{\psi}_{2,1}(x+e_1) \psi_{1,2}(x+e_1) \psi_{2,2}(x+e_1)/2 \quad (27)
 \end{aligned}$$

Vertex 20

$$\begin{aligned}
 \begin{array}{c} | \\ | \text{---} \text{---} \text{---} \\ | \end{array} &= \\
 &\left[ \begin{aligned}
 &\left[ \bar{\chi}_{1,1}(x+e_2) \bar{\psi}_{2,2}(x-e_1) + \bar{\psi}_{1,2}(x-e_1) \bar{\chi}_{2,1}(x+e_2) \right] \\
 &\times \left[ \bar{\chi}_{1,2}(x-e_2) \bar{\psi}_{2,1}(x+e_1) + \bar{\psi}_{1,1}(x+e_1) \bar{\chi}_{2,2}(x-e_2) \right] \\
 &- \left[ \bar{\psi}_{1,2}(x-e_1) \bar{\chi}_{2,2}(x-e_2) + \bar{\chi}_{1,2}(x-e_2) \bar{\psi}_{2,2}(x-e_1) \right] \\
 &\times \left[ \bar{\psi}_{1,1}(x+e_1) \bar{\chi}_{2,1}(x+e_2) + \bar{\chi}_{1,1}(x+e_2) \bar{\psi}_{2,1}(x+e_1) \right]
 \end{aligned} \right] \\
 &\times \left[ \begin{aligned}
 &\left[ \chi_{1,2}(x+e_2) \psi_{2,1}(x-e_1) + \psi_{1,1}(x-e_1) \chi_{2,2}(x+e_2) \right] \\
 &\times \left[ \chi_{1,1}(x-e_2) \psi_{2,2}(x+e_1) + \psi_{1,2}(x+e_1) \chi_{2,1}(x-e_2) \right] \\
 &- \left[ \psi_{1,1}(x-e_1) \chi_{2,1}(x-e_2) + \chi_{1,1}(x-e_2) \psi_{2,1}(x-e_1) \right] \\
 &\times \left[ \psi_{1,2}(x+e_1) \chi_{2,2}(x+e_2) + \chi_{1,2}(x+e_2) \psi_{2,2}(x+e_1) \right]
 \end{aligned} \right] / 4 \quad (28)
 \end{aligned}$$



Remarkably, as one recognizes from the above equations the remaining field combinations on the odd sublattice factorize for each vertex into exactly identical contributions from the  $\bar{\psi}$ ,  $\bar{\chi}$  and the  $\psi$ ,  $\chi$  subsystems. To see this use the map

$$\begin{aligned}\bar{\psi}_{i,1}(x) &\longleftrightarrow - - \psi_{i,2}(x) \quad , \\ \bar{\psi}_{i,2}(x) &\longleftrightarrow \psi_{i,1}(x)\end{aligned}\tag{29}$$

entailing

$$\begin{aligned}\bar{\chi}_{i,1}(x) &\longleftrightarrow \chi_{i,2}(x) \quad , \\ \bar{\chi}_{i,2}(x) &\longleftrightarrow - - \chi_{i,1}(x) \quad .\end{aligned}\tag{30}$$

The above mentioned factorization property for each vertex comes as a surprise because it could hardly have been guessed prior to the explicit calculation. The vertex factorization property immediately leads to the conclusion that any individual contribution (of any vertex cluster) to the partition function  $Z_\Lambda$  is positive. The minus sign in front of the r.h.s. of eqs. (16)-(19), (24)-(27) at first glance disturbing this property is properly taken care of by the map (29), (30). It should be mentioned that a similar vertex factorization property holds in the one-flavour Schwinger model [1], there however being fulfilled rather trivially. One might wonder, whether a vertex factorization property also holds for the strong coupling Schwinger model with a larger number of fermion species than two, perhaps being a rather general structure.

The vertex factorization property means that we can now restrict ourselves to the discussion of the  $\psi$ ,  $\chi$  subsystem. Each vertex cluster contributing to the partition function  $Z_\Lambda$  adds a term to the partition sum equal to the square of the weight of the corresponding cluster in the  $\psi$ ,  $\chi$  subsystem. We consequently need to know weights in the  $\psi$ ,  $\chi$  subsystem up to minus signs only. In order to achieve further understanding it is useful to assign the remaining  $\psi$ ,  $\chi$  fields on the odd sublattice  $\Lambda_o$  certain graphical symbols as follows (The full black dot denotes a point  $x$  on the even sublattice while the hollow circle stands for the point on the odd sublattice which the argument of the fields relates to.).

$$\circ \rightarrow \bullet = \psi_{1,1}(x - e_1) \tag{31} \quad \circ \leftarrow \bullet = \psi_{2,1}(x - e_1) \tag{32}$$

$$\bullet \rightarrow \circ = \psi_{2,2}(x + e_1) \tag{33} \quad \bullet \leftarrow \circ = \psi_{1,2}(x + e_1) \tag{34}$$

$$\begin{array}{c} \bullet \\ | \\ \circ \end{array} = \chi_{1,1}(x - e_2) \quad (35) \quad \begin{array}{c} \bullet \\ | \\ \circ \end{array} = \chi_{2,1}(x - e_2) \quad (36)$$

$$\begin{array}{c} \circ \\ | \\ \bullet \end{array} = \chi_{2,2}(x + e_2) \quad (37) \quad \begin{array}{c} \circ \\ | \\ \bullet \end{array} = \chi_{1,2}(x + e_2) \quad (38)$$

As a rule, an arrow flowing out of a point of the odd sublattice (hollow circles) denotes a field with flavour index 1 while an arrow flowing into a point on the odd sublattice relates to a field with flavour index 2. From this it is already clear that only those products of (four) Grassmann fields at any point of the odd sublattice allow non-vanishing contributions to the partition function  $Z_\Lambda$  which have two incoming and two outgoing arrows in their graphical symbols. We will refer to this fact as the vertex arrow rule. The symbols for the fields on the odd sublattice can now be used in a natural way to construct further graphical building blocks.

$$\begin{array}{c} \circ \\ | \\ \bullet \\ | \\ \circ \end{array} = \begin{array}{c} \circ \\ | \\ \bullet \\ | \\ \bullet \\ | \\ \circ \end{array} + \begin{array}{c} \circ \\ | \\ \bullet \\ | \\ \bullet \\ | \\ \circ \end{array} \\ = \chi_{1,1}(x - e_2) \chi_{2,2}(x + e_2) + \chi_{1,2}(x + e_2) \chi_{2,1}(x - e_2) \quad (39)$$

$$\begin{array}{c} \circ \text{---} \bullet \text{---} \circ \end{array} = \begin{array}{c} \circ \text{---} \bullet \text{---} \bullet \text{---} \circ \end{array} + \begin{array}{c} \circ \text{---} \bullet \text{---} \bullet \text{---} \circ \end{array} \\ = \psi_{1,1}(x - e_1) \psi_{2,2}(x + e_1) + \psi_{1,2}(x + e_1) \psi_{2,1}(x - e_1) \quad (40)$$

$$\begin{array}{c} \bullet \text{---} \circ \\ | \\ \circ \end{array} = \begin{array}{c} \bullet \text{---} \bullet \text{---} \circ \\ | \\ \circ \end{array} + \begin{array}{c} \bullet \text{---} \bullet \text{---} \circ \\ | \\ \circ \end{array} \\ = \chi_{1,1}(x - e_2) \psi_{2,2}(x + e_1) + \psi_{1,2}(x + e_1) \chi_{2,1}(x - e_2) \quad (41)$$

$$\begin{array}{c} \circ \\ | \\ \bullet \text{---} \circ \end{array} = \begin{array}{c} \circ \\ | \\ \bullet \text{---} \bullet \end{array} + \begin{array}{c} \circ \\ | \\ \bullet \text{---} \bullet \end{array} \\ = \psi_{1,1}(x - e_1) \chi_{2,2}(x + e_2) + \chi_{1,2}(x + e_2) \psi_{2,1}(x - e_1) \quad (42)$$

$$\begin{aligned}
\begin{array}{c} \circ \\ | \\ \bullet \text{---} \circ \end{array} &= \begin{array}{c} \circ \\ | \\ \bullet \text{---} \bullet \end{array} + \begin{array}{c} \circ \\ | \\ \bullet \leftarrow \bullet \end{array} \\
&= \chi_{1,2}(x + e_2) \psi_{2,2}(x + e_1) + \psi_{1,2}(x + e_1) \chi_{2,2}(x + e_2) \quad (43)
\end{aligned}$$

$$\begin{aligned}
\begin{array}{c} \circ \text{---} \bullet \\ | \\ \circ \end{array} &= \begin{array}{c} \circ \text{---} \bullet \\ | \\ \bullet \end{array} + \begin{array}{c} \circ \text{---} \bullet \\ | \\ \bullet \end{array} \\
&= \psi_{1,1}(x - e_1) \chi_{2,1}(x - e_2) + \chi_{1,1}(x - e_2) \psi_{2,1}(x - e_1) \quad (44)
\end{aligned}$$

$$\begin{array}{c} \bullet \\ | \\ \circ \end{array} = \begin{array}{c} \bullet \\ | \\ \circ \end{array} \times \begin{array}{c} \bullet \\ | \\ \circ \end{array} = \chi_{1,1}(x - e_2) \chi_{2,1}(x - e_2) \quad (45)$$

$$\begin{array}{c} \circ \\ | \\ \bullet \end{array} = \begin{array}{c} \circ \\ | \\ \bullet \end{array} \times \begin{array}{c} \circ \\ | \\ \bullet \end{array} = \chi_{1,2}(x + e_2) \chi_{2,2}(x + e_2) \quad (46)$$

$$\begin{array}{c} \circ \text{---} \bullet \end{array} = \begin{array}{c} \circ \text{---} \bullet \end{array} \times \begin{array}{c} \circ \text{---} \bullet \end{array} = \psi_{1,1}(x - e_1) \psi_{2,1}(x - e_1) \quad (47)$$

$$\begin{array}{c} \bullet \text{---} \circ \end{array} = \begin{array}{c} \bullet \leftarrow \circ \end{array} \times \begin{array}{c} \bullet \rightarrow \circ \end{array} = \psi_{1,2}(x + e_1) \psi_{2,2}(x + e_1) \quad (48)$$

Using above pictorial language for the remaining fields and their combinations on the odd sublattice we can gain now already some intuitive understanding for the structures appearing on the r.h.s. of eqs. (11)-(26). We give some characteristic examples, similar relations can also be obtained for the vertices omitted now. Please note, that the symbols on the l.h.s. below stand for the original expressions (11), (14), (18), (22), (28) restricted to the  $\psi, \chi$  factors (The numerical factors have been included with their roots, therefore.).

Vertex 3

$$\begin{array}{c} | \\ \text{---} \\ | \end{array} = \begin{array}{c} \circ \rightarrow \bullet \rightarrow \circ \end{array} \times \begin{array}{c} \circ \leftarrow \bullet \leftarrow \circ \end{array} = - \begin{array}{c} \circ \text{---} \bullet \end{array} \times \begin{array}{c} \bullet \text{---} \circ \end{array} \quad (49)$$

Vertex 6

$$\begin{array}{c} | \\ \text{---} \\ | \end{array} = \frac{1}{2} \begin{array}{c} \circ \\ | \\ \bullet \text{---} \circ \end{array} \times \begin{array}{c} \circ \\ | \\ \bullet \text{---} \circ \end{array} = -\frac{1}{2} \begin{array}{c} \circ \\ | \\ \bullet \end{array} \times \begin{array}{c} \bullet \text{---} \circ \end{array} \quad (50)$$

Vertex 10

$$\begin{array}{c} | \\ \hline \vdots \end{array} = -\frac{1}{2} \begin{array}{c} \circ \\ | \\ \bullet \end{array} \times \begin{array}{c} \circ \\ | \\ \bullet \end{array} = \frac{1}{2} \begin{array}{c} \circ \\ | \\ \bullet \end{array} \times \begin{array}{c} \circ \\ | \\ \bullet \end{array} \quad (51)$$

Vertex 14

$$\begin{array}{c} | \\ \hline \bullet \end{array} = \frac{-1}{\sqrt{2}} \begin{array}{c} \circ \\ | \\ \bullet \end{array} \times \begin{array}{c} \circ \\ | \\ \bullet \end{array} = \frac{1}{\sqrt{2}} \begin{array}{c} \circ \\ | \\ \bullet \end{array} \times \begin{array}{c} \bullet \\ \hline \circ \end{array} \quad (52)$$

Vertex 20

$$\begin{array}{c} | \\ \hline \bullet \\ \hline | \end{array} = \frac{1}{2} \begin{array}{c} \circ \\ | \\ \bullet \end{array} \times \begin{array}{c} \bullet \\ \hline \circ \end{array} - \frac{1}{2} \begin{array}{c} \circ \\ | \\ \bullet \end{array} \times \begin{array}{c} \circ \\ | \\ \bullet \end{array} \quad (53)$$

One immediately recognizes the significance of the numerical factors for each vertex. The rule simply is that each corner element (41)-(44) is associated with a factor  $1/\sqrt{2}$ . Although more useful at the end, in this respect the graphical representations given rightmost in eqs. (50), (51) are somewhat misleading.

What remains to be done now is to discuss the result for the Grassmann integration on the odd sublattice. For the moment we exclude vertex 20 (and its equivalent on the odd sublattice) from the consideration as its complexity requires special attention. It will be discussed at a later stage. In view of the vertex arrow rule one finds the following non-zero results (We give only few typical cases, all others are related by symmetry considerations of the pictures using rotations and reflections.). The graphical symbols below denote in an intuitive way the product of (four) Grassmann variables, their ordering performed clockwise with respect to the points on the even sublattice starting with the leftmost point in a picture. The black dot in the hollow circle of the point on the odd sublattice indicates that the Grassmann integration has been performed now.

$$\begin{array}{c} \bullet \\ \hline \bullet \end{array} = \int \prod_{i=1}^2 \prod_{\alpha=1}^2 d\psi_{i,\alpha}(x) \psi_{1,2}(x) \psi_{2,2}(x) \psi_{1,1}(x) \psi_{2,1}(x) = -1 \quad (54)$$

$$\begin{array}{c} \bullet \\ | \\ \bullet \end{array} = -\frac{1}{2} \quad (55)$$

$$\begin{array}{c} \bullet \\ | \\ \bullet \leftarrow \bigcirc \rightarrow \bullet \\ | \\ \bullet \end{array} = - \begin{array}{c} \bullet \\ | \\ \bullet \rightarrow \bigcirc \leftarrow \bullet \\ | \\ \bullet \end{array} = \frac{1}{2} \quad (56)$$

$$\begin{array}{c} \bullet \\ | \\ \bullet \rightarrow \bigcirc \leftarrow \bullet \\ | \\ \bullet \end{array} = - \begin{array}{c} \bullet \\ | \\ \bullet \leftarrow \bigcirc \rightarrow \bullet \\ | \\ \bullet \end{array} = \frac{1}{\sqrt{2}} \quad (57)$$

From these results one recognizes that links with  $k_l = 1$  (thin lines) must form self-avoiding loops. It remains to determine the weight of such loops inasmuch as vertices contributing to such loops have two terms each (see, e.g., eqs. (51), (52) and (40), (42)). However, due to the vertex arrow rule only those products of terms give a non-vanishing contribution which form an oriented loop. This leaves for each loop just two terms (corresponding to the two possible orientations of the loop). Both of these terms give exactly the same contribution. This can be seen easily by interchanging flavours 1 and 2 what amounts to arrow reversal. Each of the building blocks of a thin line ( $k_l = 1$ ) loop (40)-(44) transforms under flavour exchange into the negative of itself. Also, in view of eqs. (56), (57) at each point belonging to the odd sublattice of a given thin line loop arrow reversal brings a relative minus sign about. Now, these two minus signs match locally at each point of the odd sublattice of a given thin line loop. Consequently, the weight of each thin line loop is given by the product of the weights of its constituting vertices multiplied by a factor of 2 (the loop multiplicity). Finally, one recognizes from eqs. (55)-(57) that each corner (being the product of 2 fields originally) contributes a factor of  $1/\sqrt{2}$  (For eq. (56) one has to apply an interpretation analogous to the middle part of eq. (51), of course.).

Let us now extend the analysis by also allowing configurations containing vertex 20 we omitted so far. It is clear from the beginning that the picture of self-avoiding thin line ( $k_l = 1$ ) loops cannot be maintained in any naive way, but we will see how it can still be used in a modified version. The above expression (53) already suggests what can be done. One may identify the vertex 20 with two loop segments passing each other in a given point without intersection. Clearly, there are two ways of doing so which are reflected in the two different terms shown in eq. (53). Each of these two terms corresponds to four possible combinations of segments of oriented loops (each being related to the product of four fields on the odd sublattice, cf. eqs. (41)-(44)). If the two segments happen to be just different parts of one loop two of the four possible combinations of oriented thin line loop segments are effective in the final Grassmann integration over the odd sublattice only (The other two combinations must then lead to a zero result according to the vertex arrow rule.). If they belong to two different loops all terms contribute at the end. In considering the two terms in eq. (53), it is clear however that, if one term is part of two different

loops, the other must just belong to one loop returning at some stage to the point  $x \in \Lambda_e$  under consideration. Consequently, the two terms in eq. (53) differ in their contribution at the end just by a factor of 2 if it comes to the loop count (just for geometrical reasons). As each self-avoiding loop contributes a factor of 2 (related to the two different orientations of the loop) the term which is part of two different loops will be related to a factor of 4 while the other one is related to a factor of 2 only. The remaining worry is what can be said with respect to the relative sign of the contributions from the two terms in eq. (53). We will see that the relative minus sign in eq. (53) is spurious (arising from ordering effects of Grassmann variables) and that in fact the contributions from the two terms in eq. (53) add up at the end. This can be detected by noting that if one writes the two geometrically different terms in eq. (53) as sum over products of (four) fields two of these products are the same, namely  $\psi_{1,1}(x - e_1) \chi_{2,2}(x + e_2) \psi_{1,2}(x + e_1) \chi_{2,1}(x - e_2)$  (The horizontal arrows are flowing in into the point  $x$  while the vertical ones are flowing out.) and  $\psi_{2,1}(x - e_1) \chi_{1,2}(x + e_2) \psi_{2,2}(x + e_1) \chi_{1,1}(x - e_2)$  (The horizontal arrows are flowing out of the point  $x$  while the vertical ones are flowing in.). Both contribute to the l.h.s. of eq. (53) with a total factor of 1 at the end. This proves that contributions from both terms in eq. (53) add up after properly taking into account ordering effects.

Finally, to complete the picture we have to discuss the analogue of vertex 20 on the odd sublattice. One finds the following non-vanishing Grassmann integrals beyond those given in eqs. (54)-(57) (We apply here the same conventions as there.).

$$\begin{array}{c} \bullet \\ | \\ \bullet \rightarrow \bigcirc \leftarrow \bullet \\ | \\ \bullet \end{array} = \begin{array}{c} \bullet \\ | \\ \bullet \leftarrow \bigcirc \rightarrow \bullet \\ | \\ \bullet \end{array} = -1 \quad (58)$$

$$\begin{array}{c} \bullet \\ | \\ \bullet \rightarrow \bigcirc \leftarrow \bullet \\ | \\ \bullet \end{array} = \begin{array}{c} \bullet \\ | \\ \bullet \leftarrow \bigcirc \rightarrow \bullet \\ | \\ \bullet \end{array} = \begin{array}{c} \bullet \\ | \\ \bullet \rightarrow \bigcirc \leftarrow \bullet \\ | \\ \bullet \end{array} = \begin{array}{c} \bullet \\ | \\ \bullet \leftarrow \bigcirc \rightarrow \bullet \\ | \\ \bullet \end{array} = \frac{1}{2} \quad (59)$$

Again, the loop picture is helpful to recognize the underlying structure. Each of the vertices given in eq. (59) allows in an unique way an interpretation as standing for two segments of oriented loops passing each other in the given point on the odd sublattice without intersection (The first two diagrams are standing in correspondence to the first term in eq. (53) while the other two are being analogous to the second term in eq. (53).). This interpretation is supported by the appearance of the factor 1/2 (characteristic for two corners) on the r.h.s. of eq. (59). Arrow reversal for just one loop corner transforms any diagram of eq. (59) into one of the diagrams shown in eq. (58). This immediately sheds light onto the different numerical result for these. We may imagine each diagram in eq. (58) being a sum of two identical terms each

of which is supplied with an additional specification. The additional specification is provided by one of the two possible ways of two oriented loop segments passing each other without intersection in the given lattice site (The point is that the diagrams in eq. (58) in opposition to those in eq. (59) allow two different interpretations each.). Each of those terms with the additional specification contributes  $-1/2$  then. In analogy with eq. (57), under arrow reversal for just one oriented loop corner we have obtained this way a partner for each diagram in eq. (59). This partner diagram has as weight the negative of the corresponding diagram in eq. (59). This completes the discussion.

The above consideration allows us to use the following efficient graphical rule to determine the weight of any cluster containing vertex 20 (and its analogue on the odd sublattice).

$$\begin{array}{c} | \\ \hline | \\ \hline | \end{array} \quad \longrightarrow \quad \begin{array}{c} | \\ \hline \text{---} \\ \hline | \end{array} \quad + \quad \begin{array}{c} | \\ \hline \text{---} \\ \hline | \end{array} \quad (60)$$

In words, the rule shown above simply requires to replace any vertex 20 (and its analogue on the odd sublattice) within a given cluster by two vertices built of two thin line loop segments passing each other without intersection. This leads to  $2^n$  different cluster configurations when  $n$  is the number of times vertex 20 (and its analogue on the odd sublattice) occurs in the original configuration. The investigation of the  $\psi$ ,  $\chi$  subsystem shows that this rule can reproduce the contribution of vertex 20 (and its analogue on the odd sublattice) if one assigns each of the two new vertices a factor  $1/2$ , counts any thin line ( $k_l = 1$ ) loop in the newly created configurations with a factor (loop multiplicity) of 2 (characteristic for oriented loops), and then adds up the weights of all these configurations. As the loop count gives different results in a given geometrical situation for the two vertices appearing on the r.h.s. of eq. (60) the generalization of the above rule to the whole  $\bar{\psi}$ ,  $\bar{\chi}$ ,  $\psi$ ,  $\chi$  system requires further thought. As the rule (60) can be applied for the  $\bar{\psi}$ ,  $\bar{\chi}$  and the  $\psi$ ,  $\chi$  subsystems separately each occurrence of a vertex 20 (and its analogue on the odd sublattice) leads to a situation where it is met twice in a product of field combinations related to this lattice site as one recognizes from the picture below (The vertices of the  $\bar{\psi}$ ,  $\bar{\chi}$  subsystem (upper line) are emphasized by stronger lines. If one wants to have in mind some explicit expression for the intuitive picture below, eq. (53) is recommended as reference.).

$$\begin{aligned}
& \left( \begin{array}{c} | \\ \text{---} \text{---} \\ | \end{array} + \begin{array}{c} | \\ \text{---} \text{---} \\ | \end{array} \right) \\
\times & \left( \begin{array}{c} | \\ \text{---} \text{---} \\ | \end{array} + \begin{array}{c} | \\ \text{---} \text{---} \\ | \end{array} \right) \tag{61}
\end{aligned}$$

There does not exist any problem connected with the two terms where the vertices are identical in the  $\bar{\psi}, \bar{\chi}$  and the  $\psi, \chi$  subsystems. However, there are also two cross terms which have to be taken care of. In principle, it would be our aim to apply the rule (60) to the complete  $\bar{\psi}, \bar{\chi}, \psi, \chi$  system by simply changing the thin line loop multiplicity from 2 (for each subsystem) to 4 (for the complete system) but these cross terms prevent us from doing so. Consequently, if one wants to determine the weight of a given cluster for the full  $\bar{\psi}, \bar{\chi}, \psi, \chi$  system one has to carry out the loop count for one subsystem with loop multiplicity 2 and then to square the result to get the correct final weight. The study of some simple clusters suggests that one might be able to simplify this procedure by redefining the weights of the two vertices on the r.h.s. of eq. (60) (i.e., by hiding the contribution of the two cross terms in eq. (61) in a modified weight for the two terms where the vertices are identical in the  $\bar{\psi}, \bar{\chi}$  and  $\psi, \chi$  subsystems). However, closer inspection reveals that such a simplification is not possible.

We are now in a position to characterize the vertex model equivalent to the two-flavour strong coupling lattice Schwinger model with Wilson fermions. It is a (modified) 3-state 20-vertex model on the square lattice. The vertices are shown in Fig. 1 and the vertex weights are given below. (All other vertices of the 3-state model one might think of have vanishing weight.). The term 3-state refers to the three possible states of links ( $k_l = 0, 1, 2$ ; dashed, thin and thick lines respectively).

$$\omega_1 = z = \frac{1}{16\kappa_1^2\kappa_2^2} = M_1^2 M_2^2 \tag{62}$$

$$\omega_2 = \omega_3 = 1 \tag{63}$$

$$\omega_4 = \omega_5 = \omega_6 = \omega_7 = \omega_8 = \omega_9 = \omega_{10} = \omega_{11} = \omega_{20} = \frac{1}{4} \tag{64}$$

$$\omega_{12} = \omega_{13} = \omega_{14} = \omega_{15} = \omega_{16} = \omega_{17} = \omega_{18} = \omega_{19} = \frac{1}{2} \tag{65}$$



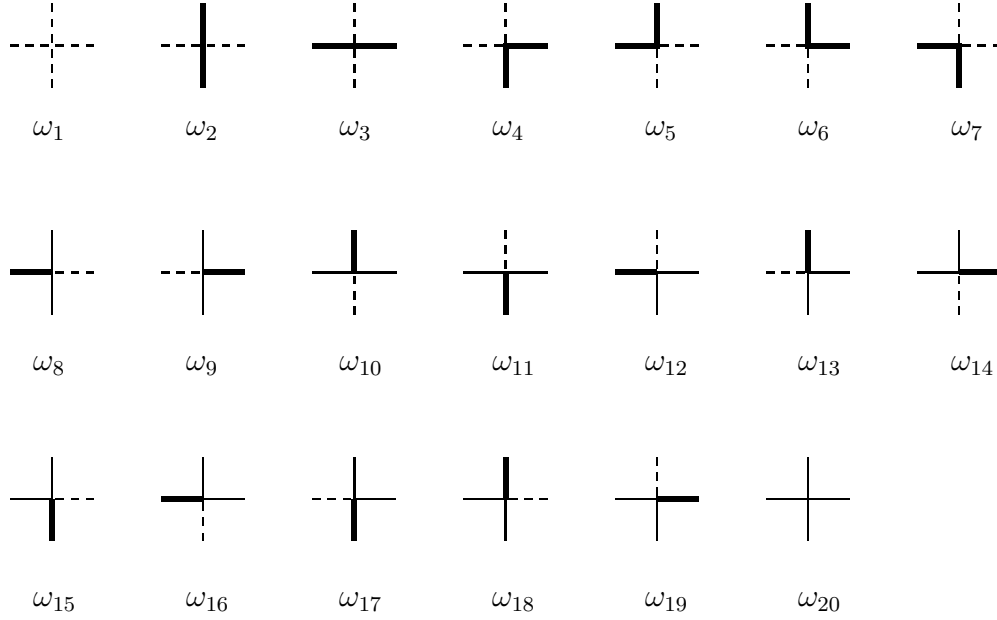


**Figure 1:** Vertices of the (modified) 3-state 20-vertex model on the square lattice equivalent to the two-flavour strong coupling Schwinger model

The partition function reads

$$Z_{\Lambda} = Z_{\Lambda}[z] = \sum_L z^{|\Lambda|-|L|} N(L)^2 \left(\frac{1}{2}\right)^{C(L)} \quad (66)$$

with

$$N(L) = \sum_{s=0} N(s, L) 2^s \quad . \quad (67)$$

The sum in eq. (66) is extended over all possible configurations  $L$  that can be built from the vertices 1-20.  $|\Lambda|$  is the number of lattice points and  $|L|$  the number of links with thin or thick lines ( $k_l = 1, 2$ ).  $C(L)$  counts the number of times a thin line bends (For the purpose of this count thick lines are understood as being equivalent to two thin lines and the vertices 8-11 therefore represent a twofold bending of a thin line. For vertex 20, we recall the rule (60).  $P_n(L)$  is the number of times the vertex  $n$  appears in a given configuration  $L$ .)

$$C(L) = 2 \sum_{n=4}^{11} P_n(L) + \sum_{n=12}^{19} P_n(L) + 2 P_{20}(L) \quad (68)$$

The factor  $1/2$  then can be understood as a bending rigidity of thin lines. The same factor for the bending rigidity has been found in the one-flavour strong coupling Schwinger model [1].  $N(s, L)$  is the number of configurations with  $s$  thin line loops generated from  $L$  by application of the rule (60). Following sum rule of course holds.

$$\sum_{s=0} N(s, L) = 2^{P_{20}(L)} \quad (69)$$

If  $P_{20}(L) = 0$ , one finds therefore

$$N(L)^2 = 4^{S(L)} \quad (70)$$

where  $S(L)$  denotes the number of thin line loops in a given configuration  $L$ . In this simple case, thin line loops enter with a multiplicity of 4 (This case bears some similarity to the general loop model discussed in [8].).

Eq. (66) defines a modified 3-state model because in the usual definition of a 3-state model the factor  $N(L)^2$  would not be present. Q-state models with certain similarities to eq. (66) (without the factor  $N(L)^2$ ) have been investigated e.g. in [9]-[18]. For  $z = 0$  we obtain a 19-vertex model. Somewhat similar 19-vertex models (without the factor  $N(L)^2$ ) have recently been discussed in [19]-[21]. Now, the modified 3-state model (66) can alternatively be understood as a regular 6-state model. To see this note, that with reference to the graphical rules given above each thin line ( $k_l = 1$ ) can be considered as having 4 different states. According to eqs. (31)–(38) each thin line term considered within the  $\bar{\psi}, \bar{\chi}$  and  $\psi, \chi$  subsystems can be related to an arrow assigned to this line. This assignment leads to four different states for thin lines and transforms the 3-state model into a 6-state model. Consequently, in this picture the vertices 8-19 split into four different 6-state model vertices (each corresponds to one of the four different products of fields related to a given 3-state model vertex, cf. eqs. (16)–(27)). Each of these vertices has the weight of the corresponding 3-state model vertex. The vertex 20 yields  $6 \times 6 = 36$  different 6-state model vertices (in each subsystem the vertex 20 corresponds to 6 different products of fields only, cf. eq. (28)). The weights of the 6-state model vertices derived from the vertex 20 can easily be determined by expanding the r.h.s. of eq. (28) in terms of products of fields. Taking into account the above considerations one may conclude that the modified 3-state 20-vertex model (66) is equivalent to a regular 6-state 91-vertex model. To which extent this is actually useful information remains to be seen in the future. Another line of thought might be linked to the following consideration. As  $N(L)$  is related to some loop count the vertex model (66) bears some resemblance to a loop model. The loop model picture becomes even more obvious if one interprets thick lines in the present model as two parallel thin lines. If one then applies the

rule (60) to both the  $\bar{\psi}$ ,  $\bar{\chi}$  and the  $\psi$ ,  $\chi$  subsystems and assigns each subsystem a colour, we end up with a 2-colour loop system on the square lattice. A loop model which comes closest to this picture has been discussed in [22]. However, the relation to the present model does not go beyond a certain remote similarity.

Finally, in analogy with the one-flavour case let us discuss the critical behaviour of the two-flavour strong coupling Schwinger model by means of some approximate method. We are going to rely on a generalization of the independent loop approximation (cf. sect. 3 of [6]) which we now appropriately call independent cluster approximation. As in the case of the independent loop approximation we assume that the system under consideration is sufficiently dilute in the relevant parameter region in order to yield reasonable results. We start with the observation that any cluster built of the vertices 2-20 falls into two classes. Either we have a self-avoiding thick line loop or some cluster containing thin line segments. In the independent cluster approximation we now write the partition function  $Z_\Lambda[z]$  as follows.

$$Z_\Lambda[z] = z^{|\Lambda|} e \left\{ Z_\Lambda[1, z, 1/4] + \bar{Z}_\Lambda[1, z] \right\} \quad (71)$$

Here,  $Z_\Lambda[1, z, \eta]$  is the single loop partition function defined in sect. 3 of [6].  $\bar{Z}_\Lambda[1, z]$  denotes the single cluster partition function in which the statistical sum is extended only over all possible configurations  $L$  containing just one cluster containing thin lines.  $z^{|\Lambda|} Z_\Lambda[1, z, 1/4]$  coincides with  $Z_\Lambda[z]$  when the summation in eq. (66) is restricted to configurations  $L$  with just one thick line loop.  $z^{|\Lambda|} \bar{Z}_\Lambda[1, z]$  coincides with  $Z_\Lambda[z]$  when the summation in eq. (66) is restricted to configurations  $L$  which constitute just one cluster with thin line elements. As the free energy density  $f$  reads in the independent cluster approximation ( $\beta_T = 1/T$ )

$$\begin{aligned} \beta_T f(z) &= - \lim_{|\Lambda| \rightarrow \infty} \frac{1}{|\Lambda|} \ln Z_\Lambda[z] \\ &= - \ln z - \lim_{|\Lambda| \rightarrow \infty} \frac{Z_\Lambda[1, z, 1/4] + \bar{Z}_\Lambda[1, z]}{|\Lambda|} \end{aligned} \quad (72)$$

a phase transition can be detected by looking at each single cluster (loop) partition function separately. We do not have any information about  $\bar{Z}_\Lambda[1, z]$  but the single loop partition function  $Z_\Lambda[1, z, \eta]$  has been studied in [6]. One finds a critical line described by the equation

$$z(\eta) = 1 + \eta (\mu - 1) \quad . \quad (73)$$

$\mu = 2.638\dots$  is the effective coordination number of the square lattice. From eq. (73) one immediately obtains in the present case

$$z_{cr} = M_1^2 M_2^2 = \frac{1}{16\kappa_1^2 \kappa_2^2} = \frac{(\mu + 3)}{4} . \quad (74)$$

From the experience with the one-flavour [1] and the two-flavour strong coupling Schwinger models it seems reasonable to expect that for the investigation of the critical behaviour of the general  $N_f$ -flavour model the self-avoiding loop model with bending rigidity  $\eta = 2^{-N_f}$  will be relevant.

To conclude, we have found the vertex model equivalent to the two-flavour strong (infinite) coupling lattice Schwinger model with Wilson fermions. This demonstrates that the method employed by Salmhofer for the one-flavour case [1] can successfully be generalized (with some technical effort) to models with a higher number of Grassmann variables per lattice site (8 in the present case; incidentally note that one-flavour strong coupling lattice QED with Wilson fermions in 4D has the same number of Grassmann variables per lattice site). As the method can also be applied to purely fermionic models this suggests a number of interesting directions for further research which will be explored in the future.

## Acknowledgements

The present work has been performed under the EC Human Capital and Mobility Program, contract no. ERBCHBGCT930470. I would like to thank Simon Hands for discussions and a critical reading of the draft version of the paper, and Holger Perlit for valuable advice concerning Mathematica.

## References

- [1] M. Salmhofer; Nucl. Phys. **B 362**(1991)641.
- [2] P. Rossi, U. Wolff; Nucl. Phys. **B 248**(1984)105.
- [3] H. Gausterer, C.B. Lang; Phys. Lett. **B 341**(1994)46.
- [4] F. Karsch, E. Meggiolaro, L. Turko; Phys. Rev. **D 51**(1995)6417.
- [5] H. Gausterer, C.B. Lang; Nucl. Phys. **B 455**[FS](1995)785.
- [6] K. Scharnhorst; University of Wales, Swansea, Preprint SWAT/95/72, hep-lat/9505001.
- [7] Wolfram Research; Mathematica, version 2.2. Wolfram Research, Champaign, 1994.
- [8] F.S. Rys, W. Helfrich; J. Phys. **A 15**(1982)599.
- [9] Yu.G. Stroganov; Phys. Lett. **A 74**(1979)116.
- [10] J.H.H. Perk, C.L. Schultz; Phys. Lett. **A 84**(1981)407.
- [11] J.H.H. Perk, C.L. Schultz, in: M. Jimbo, T. Miwa (Eds.): Non-linear Integrable Systems — Classical Theory and Quantum Theory, Proc. of RIMS Symposium organised by M. Sato, Kyoto, Japan, 13-16 May 1981. World Scientific, Singapore, 1983, p. 135.
- [12] K. Sogo, Y. Akutsu, T. Abe; Prog. Theor. Phys. **70**(1983)730, *ibid.* 739.
- [13] J.H.H. Perk, C.L. Schultz; Physica **A 122**(1983)50.
- [14] J.H.H. Perk, F.Y. Wu; Physica **A 138**(1986)100.
- [15] H.J. Giacomini; Phys. Lett. **A 117**(1986)381.
- [16] Y. Akutsu, M. Wadati; J. Phys. Soc. Jpn. **56**(1987)3039.
- [17] L.H. Gwa, F.Y. Wu; J. Phys. **A 24**(1991)L503.
- [18] M.T. Batchelor, J. Suzuki; J. Phys. **A 26**(1993)L729.
- [19] M. Idzumi, T. Tokihiro, M. Arai; J. Phys. I France **4**(1994)1151.
- [20] Y.M.M. Knops, B. Nienhuis, H.J.F. Knops, H.W.J. Blöte; Phys. Rev. **B 50**(1994)1061.

- [21] A. Klümper, S.I. Matveenko, J. Zittartz; Z. Phys. **B 96**(1995)401.
- [22] S.O. Warnaar, B. Nienhuis; J. Phys. **A 26**(1993)2301.